Electronic structure of the heavy-fermion caged compound $Ce_3Pd_{20}X_6$ (X = Si, Ge) studied by density functional theory and photoelectron spectroscopy

Hitoshi Yamaoka,[1,*] Eike F. Schwier,[2,†] Masashi Arita,[2] Kenya Shimada,[2] Naohito Tsujii,[3] Ignace Jarrige,[4] Jian Jiang,[5] Hirokazu Hayashi,[5] Hideaki Iwasawa,[2] Hirofumi Namatame,[2,5] Masaki Taniguchi,[2,5] and Hideaki Kitazawa[3]

[1]*RIKEN SPring-8 Center, RIKEN, 1-1-1 Kouto, Sayo, Hyogo 679-5148, Japan*

[2]*Hiroshima Synchrotron Radiation Center, Hiroshima University, Higashi-Hiroshima, Hiroshima 739-0046, Japan*

[3]*Quantum Beam Center, National Institute for Materials Science, 1-2-1 Sengen, Tsukuba 305-0047, Japan*

[4]*National Synchrotron Light Source II, Brookhaven National Laboratory, Upton, New York 11973-5000, USA*

[5]*Graduate School of Science, Hiroshima University, Higashi-Hiroshima, Hiroshima 739-0046, Japan*

(Received 28 October 2014; revised manuscript received 6 February 2015; published 30 March 2015)

The electronic structure of $Ce_3Pd_{20}X_6$ (X = Si, Ge) has been studied using detailed density functional theory (DFT) calculations and high-resolution photoelectron spectroscopy (PES) measurements. The orbital decomposition of the electronic structure by DFT calculations indicates that Ce atoms at the (8c) site surrounded by 16 Pd atoms have a tendency to be magnetic. Ce atoms at the (4a) site surrounded by 12 Pd and 6 X atoms, on the other hand, are more localized and paramagnetic. The $4d$-$4f$ resonance PES measurements clearly indicate the Ce $4f$ contribution in the valence band in these compounds. The spectral weight of Ce $4f^0$ is stronger than that of Ce $4f^1$, indicating the localized nature of Ce $4f$ electrons. Near the Fermi level, the Ce $4f^1$ weight of $Ce_3Pd_{20}Si_6$ is stronger than that of $Ce_3Pd_{20}Ge_6$, suggesting stronger c-f hybridization in the former.

DOI: 10.1103/PhysRevB.91.115139 PACS number(s): 79.60.−i, 71.15.Mb, 71.27.+a, 75.20.Hr

I. INTRODUCTION

The caged compound $Ce_3Pd_{20}Si_6$ is known to be one of the heaviest electron Kondo systems, with a low-temperature electronic specific heat coefficient of $\gamma = 8$ J/mol K^2 [1,2]. Such a large γ value is normally attributed to strong electron correlations and a high density of states (DOS) at the Fermi level (E_F). $Ce_3Pd_{20}Si_6$ has a characteristic geometric structure: Pd and Si atoms form cages which accommodate Ce guest ions. The family of $R_3Pd_{20}X_6$ (R = La, Ce; X = Si, Ge) compounds is a potential candidate for thermoelectric applications, having a large thermoelectric figure of merit, which is derived from the rattling motion of guest atoms in the cage structure [3–8]. Furthermore, it has attracted much interest that quantum criticality might be achieved in $Ce_3Pd_{20}Si_6$ by hydrostatic pressure, chemical pressure, and magnetic field [6–10].

In $Ce_3Pd_{20}Si_6$ Ce atoms occupy two crystallographic sites, (8c) and (4a), which are surrounded by 16 Pd atoms and 12 Pd and 6 Si atoms, respectively [11]. With decreasing temperature a quadrupole order at $T_Q = 0.52$ K at the (8c) site [12] and antiferromagnetic order at $T_N = 0.33$ K at the (4a) site [13] occurred and both orders coexist at low temperature. The temperature dependence of the resistivity showed a typical behavior due to incoherent Kondo scattering [1,5]. Its maximum corresponds to the onset of Kondo screening at the Kondo temperature $T_K \approx 20$ K. It was suggested that Ce at the (4a) site determined the Kondo properties, while Ce at the (8c) site is responsible for the unusual magnetic behavior [14,15]. The magnetic susceptibility was Curie-Weiss like above 100 K, with an effective magnetic moment close to the theoretical value of $2.54\mu_B$ based on Hund's rule [1]. Therefore Ce in the cage was expected to be nearly in a Ce^{3+} state at high temperatures. All this resulted in a complex magnetic phase diagram [12,13,16,17]. Under a magnetic field the resistivity showed a linear temperature dependence in the range between 0.1 and 0.6 K [4]. This non-Fermi liquid behavior signaled a field-induced quantum critical point [3,6,18]. Thus $Ce_3Pd_{20}Si_6$ underwent a quantum phase transition triggering the Kondo breakdown, under a magnetic field with decreasing T_N and increasing T_Q [19]. The pressure effect on the transport properties was also studied, showing characteristic features of these Kondo compounds for the Hall constant and the electrical resistivity [9]. However, the specific heat showed little pressure dependence. To explain the contrasting behavior, two Kondo temperatures for each Ce site were considered. The crystal-field (CF) effect is also important to understand the magnetic properties. Neutron diffraction [20] and ultrasonic measurements [12] showed a Γ_7 doublet ground state for the (4a) site and Γ_8 for the (8c) site.

On the other hand, the isostructural germanide compound $Ce_3Pd_{20}Ge_6$ is a heavy-electron system with a Kondo temperature of a few kelvins [2]. The electronic specific heat coefficient of $\gamma \sim 0.7$ J/mol K^2 was smaller by one order of magnitude compared to that of $Ce_3Pd_{20}Si_6$ and the effective moment is nearly equal to that of free trivalent Ce^{3+} [2] and therefore comparable to that in $Ce_3Pd_{20}Si_6$. In $Ce_3Pd_{20}Ge_6$, similarly to $Ce_3Pd_{20}Si_6$, $T_Q = 1.2$ K and $T_N = 0.75$ K were reported [21]. A μSR study indicated that Ce ions at the (4a) site played a major role in Kondo-like behavior [22] similarly to $Ce_3Pd_{20}Si_6$. The local density approximation calculation for $La_3Pd_{20}Ge_6$ including the relativistic effect with the spin-orbit interaction showed stronger mixing effects at the (4a) site than compared to the (8a) site [23]. Under pressure T_N and T_Q did not change up to 0.3 GPa [24]. Ultrasonic experiments showed an off-center rattling motion of the Γ_5 type at the (4a) site [25]. Thermally activated rattling of the Ce ion over an anharmonic potential in a cage was observed for the Ge compound but not for the Si system [25,26]. For $Ce_3Pd_{20}X_6$ (X = Si, Ge) no photoelectron spectroscopy (PES) or density functional theory

*Correspondence author: yamaoka@spring8.or.jp

†Correspondence author: schwier@hiroshima-u.ac.jp

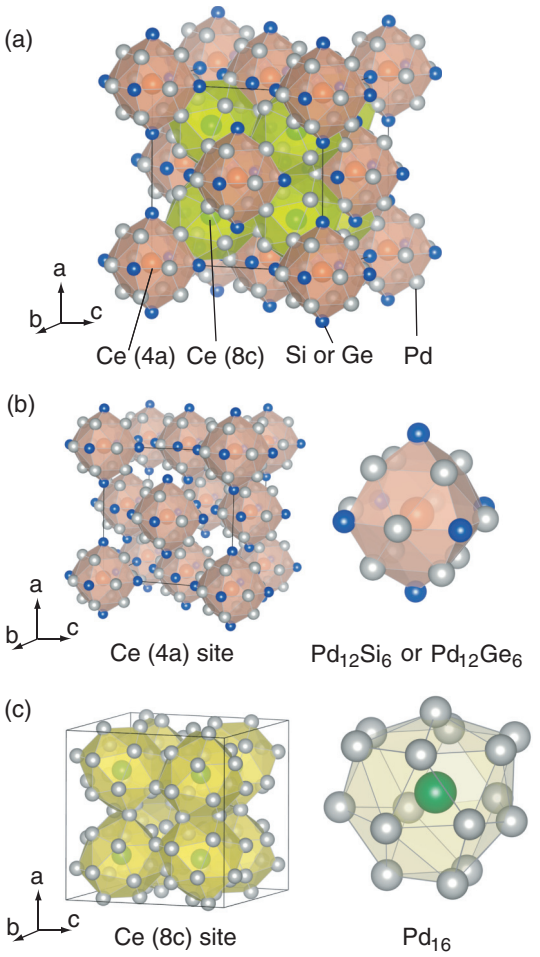

FIG. 1. (Color online) (a) Schematic image of the cubic $Cr_{22}C_6$-type crystal structure of $Ce_3Pd_{20}X_6$ (X = Si, Ge). (b) Ce_{4a} at site (4a) is surrounded by a cage of 12 Pd_{mix} and 6 Si/Ge atoms. (c) Ce_{8c} at site (8c) is inside a cage of 4 Pd_{8c} and 12 Pd_{8c} atoms.

(DFT) studies of the electronic structure have been reported so far.

In this paper we report results of DFT calculations as well as ultraviolet (UV) and soft x-ray (SX) PES measurements [27,28] for $Ce_3Pd_{20}X_6$ (X = Si, Ge). We present calculations of the electronic states of both compounds and discuss the site- and spin-resolved nature of the Pd and Ce contributions to the electronic structure. We further analyze the k- and orbital-weight-dependent band structure at E_F in order to probe the presence of c-f hybridization as well as specific differences between the two compounds. We then describe the temperature dependence of the valence band in the wide energy range and near E_F. Results from $4d$-$4f$ resonant PES in the SX energy range are also presented and Ce $4f$-derived spectra are discussed.

II. DENSITY FUNCTIONAL THEORY CALCULATIONS

A. Crystal structure

In Fig. 1 we show a schematic image of the cubic $Cr_{22}C_6$-type crystal structure (space group $Fm\bar{3}m$; No. 225) of $Ce_3Pd_{20}Si_6$ and $Ce_3Pd_{20}Ge_6$ [11]. The simple unit cell contains 116 atoms, consisting of 12 Ce, 80 Pd, and 24 X = (Si,Ge) atoms. In the primitive unit cell the number of nonequivalent atoms is reduced to 2 Ce_{8c}, 1 Ce_{4a}, 12 Pd_{mix}, and 8 Pd_{8c} as well as 6 X = (Si,Ge) atoms. While the fractional coordinates in both unit cells are identical, the lattice constants of $Ce_3Pd_{20}Ge_6$ are expanded by ~1.3% compared to those of $Ce_3Pd_{20}Si_6$ [11,21,29].

As mentioned above, Ce atoms occupy two crystallographic sites, (8c) and (4a), in the crystal structure. The two Ce_{8c} atoms at the (8c) site, with cubic T_d symmetry, are located inside a cage made up of 16 Pd atoms. These Pd atoms are classified into 4 Pd_{8c} atoms, which tetrahedrally surround the Ce_{8c} atoms with a shorter bond length, and 12 Pd_{mix} atoms, with a slightly longer distance from the Ce_{8c}. The Pd_{16} cages form a simple cubic sublattice inside the crystal. The Ce_{4a} atom at the (4a) site with cubic O_h symmetry is surrounded by a cage consisting of 12 Pd_{mix} and 6 X = (Si,Ge) atoms in a face-centered cubic sublattice. Each of the 12 Pd_{mix} atoms in the unit cell is part of three Ce cages, sharing a bond with two neighboring Ce_{8c} and one neighboring Ce_{4a} atoms. The bond length with the latter is shorter, suggesting a stronger interaction between the Pd_{mix} atoms and the Ce at the (4a) site compared to the (8c) site. We may assume that the electronic states of Pd_{8c} atoms with the shortest Ce-Pd bond length in the system are well localized within the Ce_{8c} cage.

B. Partial density of states

Taking into account the above crystal structures we performed fully relativistic DFT calculations for $Ce_3Pd_{20}X_6$ (X = Si, Ge) using the *elk* code [30], which is based on an all-electron full-potential linear augmented plane-wave (FP-LAPW) method. Exchange and correlation energies were described by the LSDA functional introduced by Perdew and Wang [31] and we used a $4 \times 4 \times 4$ Monkhorst-Pack mesh [32] centered around the L point, leading to 32 nonequivalent k points sampling the Brillouin zone. The maximum cutoff energy was 450 eV. In the beginning of the self-consistent cycle a magnetic field was applied throughout the entire unit cell in order to break the spin symmetry and allow the magnetic ground state to emerge [30].

In Fig. 2 we compare the spin- and site-integrated contributions to the DOS of $Ce_3Pd_{20}Si_6$ [Figs. 2(a)–2(d)] and $Ce_3Pd_{20}Ge_6$ [Figs. 2(e)–2(h)]. In the two most left graphs [Figs. 2(a) and 2(e)] we highlight the main contributions from each species to the DOS, namely, the Ce f, Pd d, and X = (Si,Ge) p orbitals. In the graphs (b)–(d) and (f)–(h) we have resolved the contributions of all orbitals (s, p, d, and f) from the three species inside the unit cell of $Ce_3Pd_{20}Si_6$ [Figs. 2(b)–2(d)] and $Ce_3Pd_{20}Ge_6$ [Figs. 2(f)–2(h)].

The first thing to note is the overall close resemblance of the DOS of $Ce_3Pd_{20}Si_6$ and that of $Ce_3Pd_{20}Ge_6$ as well as the overall weak contribution from X = (Si, Ge) orbitals to the electronic structure. The Ce $4f$ states are the main contributors to the conduction band and the valence band is dominated by the Pd $5d$ electrons, with some contribution from the X p electrons at higher binding energies. In the insets in Figs. 2(b) and 2(f), one can see the Ce $4f$ DOS near E_F, which is derived from the hybridization with the Pd $5d$ states (i.e., the c-f hybridization). The existence of the

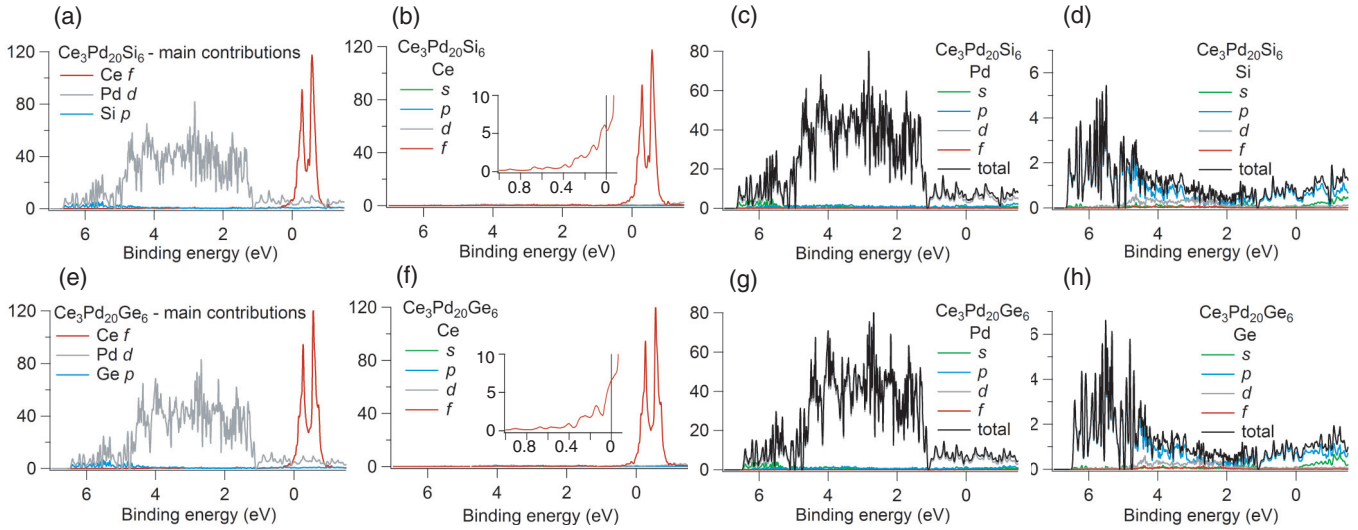

FIG. 2. (Color online) (a) Main contributions to the density of states of $Ce_3Pd_{20}Si_6$ from Ce f, Pd d, and Si p orbitals. (b–d) Partial density of states calculated within density functional theory for each species in $Ce_3Pd_{20}Si_6$. (e) Main contributions to the density of states of $Ce_3Pd_{20}Ge_6$ from Ce f, Pd d, and Ge p orbitals. (f–h) Partial density of states calculated within density functional theory for each species in $Ce_3Pd_{20}Ge_6$.

Ce $4f$ contribution below E_F is confirmed by the Ce $4d$-$4f$ resonance PES measurements.

Searching for differences between the DOS of $Ce_3Pd_{20}Si_6$ and that of $Ce_3Pd_{20}Ge_6$ we find a small shift (∼30 meV) of the valence-band maximum ($E_b \sim 1.3$ eV, where E_b is the binding energy) towards E_F. The main features in the valence band exhibit a more significant shift (∼220 meV) in the same direction. The conduction band as a whole also exhibits a small shift, ∼30 meV, again towards E_F.

To compare with the experimental results, we calculated the electronic specific heat coefficient (γ_{DFT}) using the calculated DOS at E_F. According to the Fermi liquid theory in heavy-fermion systems [33,34], the electron specific heat coefficient can be written as $\gamma^* = \frac{1}{3}\pi^2 k_B^2[\rho_c(E_F) + \frac{1}{z}\rho_f(E_F)]$, where $\rho_c(E_F)$ and $\rho_f(E_F)$ are the DOS of the conduction and f electrons at E_F, respectively. The renormalization factor z is defined by $z^{-1} = 1 - \frac{\partial \Sigma(k,\omega)}{\partial \omega}\,|_{\omega=0}$, where $\Sigma(k,\omega)$ denotes the electron self-energy. The z value gives a measure of the magnitude of electron correlation. In the case of heavy-fermion systems, the $\frac{1}{z}\rho_f(E_F)$ term mainly contributes to the enhanced γ^* value. In the absence of correlation effects ($z = 1$), the electronic specific heat coefficient based on the DFT results γ_{DFT} gives values for $Ce_3Pd_{20}Si_6$ and $Ce_3Pd_{20}Ge_6$ of ∼0.03 and ∼0.04 J/mol K^2, respectively. The experimental electronic specific heat coefficient γ_{exp} values are significantly enhanced compared with the theoretical ones, especially for $Ce_3Pd_{20}Si_6$. If we estimate z^{-1} by the ratio of $z^{-1} \sim \gamma_{\mathrm{exp}}/\gamma_{\mathrm{DFT}}$, taking into account only the f states at the Fermi level [35] we obtain $z^{-1} \sim 550$ and $z^{-1} \sim 37$ for $Ce_3Pd_{20}Si_6$ and $Ce_3Pd_{20}Ge_6$, respectively. It is noted that the electron correlation effect is significant not only for $Ce_3Pd_{20}Si_6$ but also $Ce_3Pd_{20}Ge_6$.

C. Spin- and site-resolved DOS

In Fig. 3, we plot the spin- and site-resolved DOS of the Pd_{8c} and Pd_{mix} [Fig. 3(a)] and the Ce_{8c} and Ce_{4a} [Fig. 3(b)] sites for $Ce_3Pd_{20}Si_6$ [36]. Due to the overall similarity of the

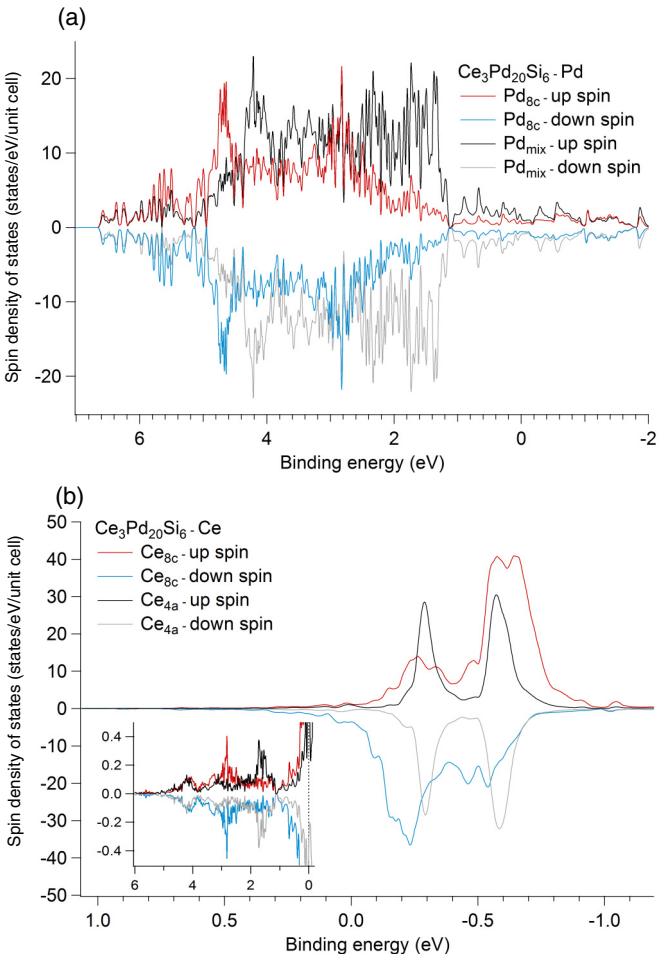

FIG. 3. (Color online) (a) Spin- and site-resolved Pd d partial density of states for $Ce_3Pd_{20}Si_6$. (b) Spin- and site-resolved Ce f partial density of states for $Ce_3Pd_{20}Si_6$.

DOS as shown in Fig. 2, we do not plot the corresponding graphs for $Ce_3Pd_{20}Ge_6$.

In Fig. 3(a) we see that Pd_{mix} dominates the low-binding-energy region of the valence band between $E_b = 1.2$ and $E_b = 2.3$ eV and has a peak at $E_b = 4.1$ eV. The Pd_{8c} states contribute to the valence band around $E_b = 2.8$ eV and $E_b = 4.7$ eV. Both species contribute states around $E_b = 5.6$, eV where the Si p states are mainly localized [see Fig. 2(d)]. Neither Pd site exhibits any spin polarization in the valence band, which is in accordance with the results from the calculation of the magnetic moment at the Pd atoms, which showed only a negligible moment.

In Fig. 3(a), the partial DOS values of Pd_{mix} are slightly larger than those of Pd_{8c} in the binding energy region $E_b = 0$–1 eV. As Pd_{mix} is shared by one (4a) and two (8c) cages, we assume that Pd d states interact with f electrons at the different sites.

It has been suggested that each Ce site plays a specific role in determining the Kondo (4a) and magnetic (8c) properties of these materials. Based on the DFT calculations, we find that Ce at the (8c) site tends to have a small magnetic moment, while Ce at the (4a) site is paramagnetic. These findings are mirrored in the PDOS of the Ce sites as shown in Fig. 3(b). Here f states in the conduction band contributed by the (8c) site are spin polarized, while states from the (4a) site are not polarized and more localized in nature. At the Fermi level, the spin-polarized f states from the (8c) site dominate compared to the contribution from the (4a) site.

D. d and f weighted band structures

In Fig. 4 we have plotted the Ce_{8c} f [Fig. 4(a)] and Pd_{8c} d [Fig. 4(b)] weighted band structure of the Pd_{16} cage as well as the Ce_{4a} f [Fig. 4(c)] and Pd_{mix} d [Fig. 4(d)] weighted band structure of the $Pd_{12}Si_6$ cage [37].

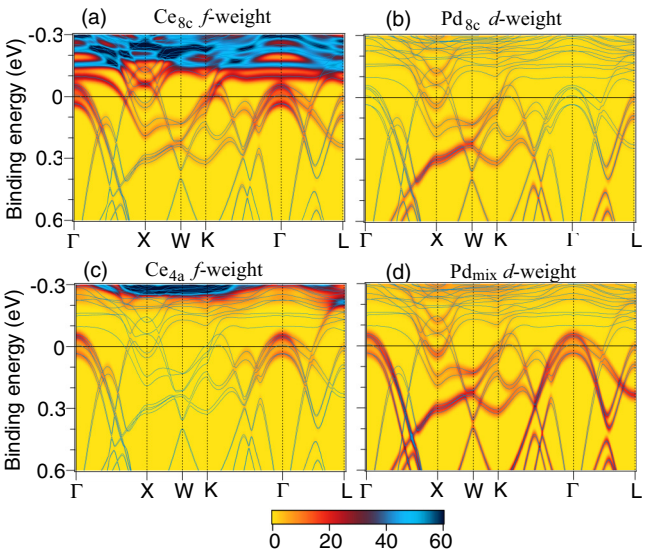

FIG. 4. (Color online) Band dispersion in the c-f hybridization of $Ce_3Pd_{20}Si_6$ weighted by the (a) Ce_{8c} f states, (b) Pd_{8c} d states, (c) Ce_{4a} f states, and (d) Pd_{mix} d states.

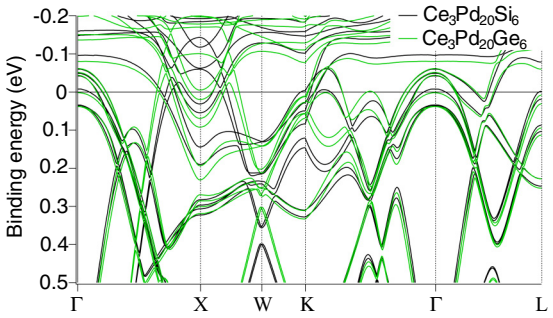

FIG. 5. (Color online) Band dispersion in the c-f hybridization of $Ce_3Pd_{20}Si_6$ (black lines) and $Ce_3Pd_{20}Ge_6$ [gray (green) lines].

In Figs. 4(a) and 4(b), for the Pd_{16} cage, which is assumed to be responsible for the magnetic properties, we see the contribution from the spin-polarized f electrons in the conduction band above $E_b = -100$ meV. The f weight is comparable irrespective of the k points in the Brillouin zone and is reduced with increasing binding energy. The Pd_{8c} d weight, on the other hand, is strongly reduced in the hole-like bands at the Γ point as well as several bands at higher binding energies near the Γ and L points.

In Figs. 4(c) and 4(d), one can see some differences in the $Pd_{12}Si_6$ cage which is assumed be responsible for the Kondo properties. The onset of the f weight is moved away from E_F. The f weight near E_F is localized in the hole pocket at the Γ point, weakly around the L point. In contrast, the Pd_{mix} d weight is more homogeneously distributed across the Brillouin zone. In particular, we now see a strong d-weight contribution at the Γ point and around the L point. We assume that these results are related to the fact that the Pd_{mix} is shared by one (4a) and two (8c) cages.

E. Comparison of the bare band structures of both compounds

In Fig. 5 we compare the unweighted band structures of $Ce_3Pd_{20}Si_6$ and $Ce_3Pd_{20}Ge_6$ at the same high-symmetry points used in the previous section. In both calculations six bands cross the Fermi level. However, for $Ce_3Pd_{20}Si_6$, four of these six form hole pockets around the Γ point and two form electron-like pockets at the X point, while $Ce_3Pd_{20}Ge_6$ has three Fermi level crossings of hole-like bands at the Γ point and three crossings of electron-like bands around the X point.

The dominance of hole pockets in $Ce_3Pd_{20}Si_6$ compared to $Ce_3Pd_{20}Ge_6$ should lead to a change in the nature of the charge carriers between the two systems. The change in the carriers should be reflected in the Hall coefficient of these compounds. For $Ce_3Pd_{20}Si_6$ the Hall coefficient showed the typical heavy-fermion behavior at high temperatures and was dominated by the normal Hall component at low temperatures [8]. Comparative measurements of the Hall coefficient for $Ce_3Pd_{20}Ge_6$ is desirable since no results have been reported, to our knowledge.

Our theoretical results may motivate de Haas–van Alphen or angle-resolved photoelectron spectroscopy (ARPES) experiments on single-crystalline samples in the future. In particular, the theoretical band structures can be directly compared with the ARPES results.

III. EXPERIMENTS

Polycrystalline $Ce_3Pd_{20}X_6$ (X = Si, Ge) samples were prepared by arc-melting stoichiometric mixtures of the pure elements (Ce:3N, Pd:3N, Si:10N, Ge:5N) in an argon gas atmosphere and subsequent annealing in an evacuated quartz tube for 120 h at 800 °C [29]. The annealed samples were examined by powder x-ray diffraction and found to be single phased.

SX and UV PES measurements were performed at the undulator beamlines BL-1 and BL-9A at the Hiroshima Synchrotron Radiation Center (HiSOR), equipped with high-resolution hemispherical electron-energy analyzers (R4000; VG-SCIENTA) [38,39]. In the UV PES the total energy resolution (ΔE) was set to be less than 20 meV at $h\nu$ = 10–20 eV and 9 K under a vacuum pressure below 2×10^{-9} Pa. In the SX PES ΔE was less than 50 meV for $h\nu = 122$ eV and 10 K with a vacuum pressure below 10^{-8} Pa. The energy resolution and the Fermi level are determined by fitting the Fermi edge of polycrystalline Au evaporated on the sample holders using a convolution of a Gaussian and the Fermi-Dirac function. All samples were fractured at a temperature of around 10 K *in situ* just before measurements.

In these compounds there are two Ce sites, which are expected to show different physical properties and temperature behaviors. Our photoemission experiment, however, averages over both Ce sites.

IV. EXPERIMENTAL RESULTS AND DISCUSSION

A. Temperature dependence

Figure 6 shows valence-band spectra in the wide binding energy range at 8–9.5 K and several incident photon energies for $Ce_3Pd_{20}Si_6$. According to the DFT calculations, the Pd 4d contribution to the valence band mainly consists of three peaks: at $E_b \sim 1.6$ eV, $E_b \sim 2.5$ eV, and $E_b \sim 4$ eV. The Pd 4d peak at $E_b \sim 2.5$ eV and $h\nu = 110$ eV splits into fine peaks at $E_b < 40$ eV because of the better resolution in the UV range. The intensity at $E_b > 5$ eV in Fig. 6(a) increases at $h\nu = 12.2$ eV due to the increase in the Si 3p photoionization cross section [40]. The DFT calculation in Fig. 6(b) corresponds well to the $h\nu$-dependent PES spectra. They mainly reflect the contribution from Pd 4d states due to the low cross sections for Ce 4f and Si 3p states.

The temperature dependence of the valence-band spectrum of $Ce_3Pd_{20}Si_6$ at $h\nu = 12.2$ eV is shown in Fig. 7. The intensity is normalized by the area at $E_b < 8.2$ eV. This incident photon energy is more bulk sensitive than the Ce 4d-4f resonance energy and thus the surface contribution is reduced. The valence-band spectra mainly reflect the Pd 4d and Si 3p DOS. Figure 7(b) shows that peaks E and D become sharper with decreasing temperature. This may be caused by the suppression of thermal broadening at low temperatures or a narrowing of the bandwidth in the valence band caused by increased electronic localization. The temperature dependence of the Fermi edge, at low photon energies, can be explained reasonably well by the Fermi-Dirac distribution function. These results indicate a very weak temperature dependence of the Pd 4d states.

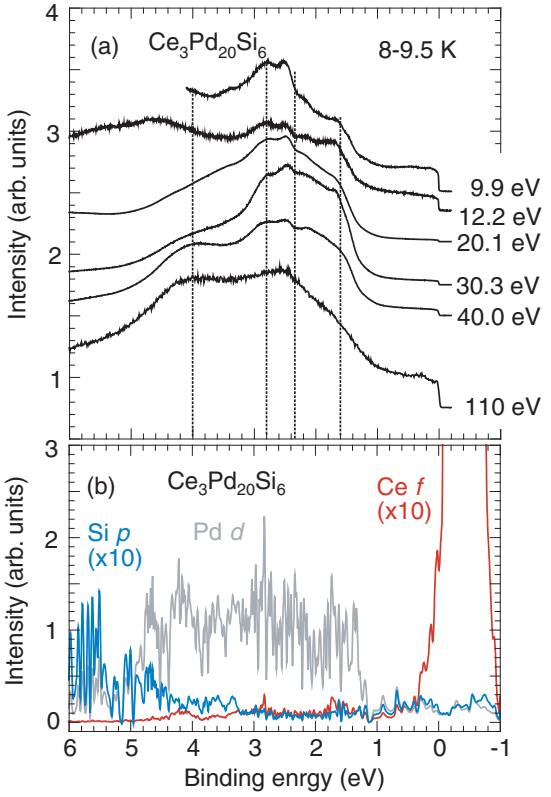

FIG. 6. (Color online) (a) Valence-band spectra near the Fermi edge at 8–9.5 K and $h\nu$ = 9.9, 12.2, 20.1, 30.3, 40, and 110 eV for $Ce_3Pd_{20}Si_6$. (b) Partial density of states calculated within DFT for $Ce_3Pd_{20}Si_6$.

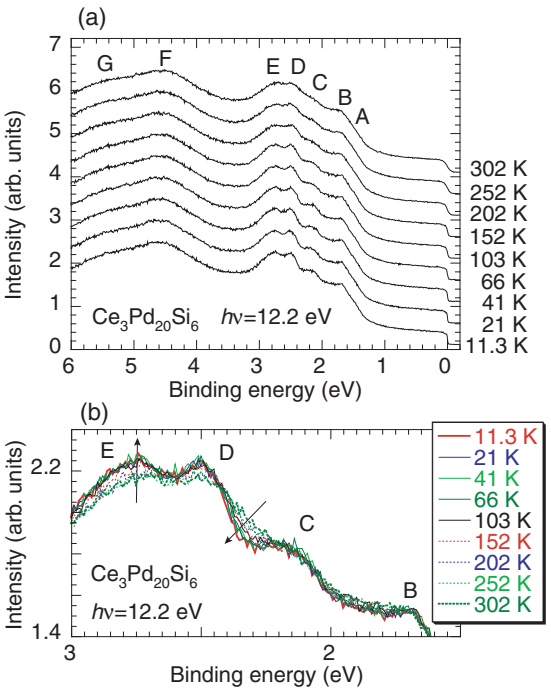

FIG. 7. (Color online) (a) Temperature dependence of the valence-band spectra at $h\nu = 12.2$ eV for $Ce_3Pd_{20}Si_6$. (b) Enlarged view of the valence-band spectra in (a) near the Fermi edge. The direction of the arrows corresponds to the change in intensity at the given binding energy when the temperature decreases.

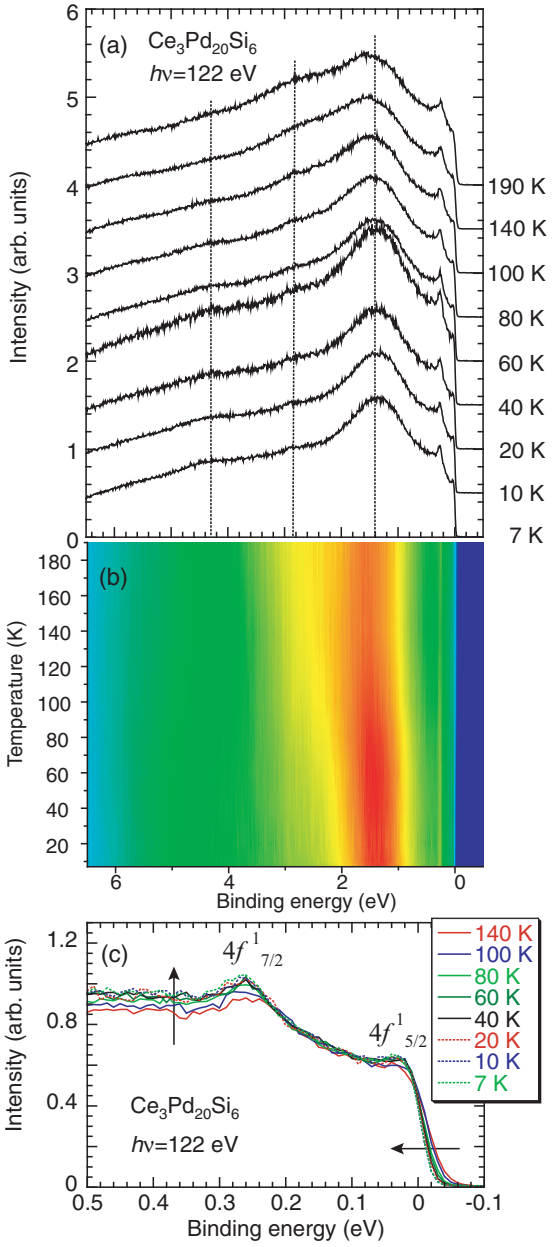

FIG. 8. (Color online) (a) Temperature dependence of the valence-band spectra at $h\nu = 122$ eV for $Ce_3Pd_{20}Si_6$. (b) Contour intensity map of the temperature dependence of the valence-band spectra in (a). (c) Enlarged view of the valence-band spectra in (a) near the Fermi edge. The direction of the arrows corresponds to the change in intensity at the given binding energy when the temperature decreases.

Figure 8 shows the temperature dependence of the valence-band spectra at $h\nu = 122$ eV, where Ce $4d$-$4f$ resonance occurs. One can clearly see the contribution of the Ce $4f$ states in the valence band, which is enhanced in the $4d$-$4f$ resonance region. Based on the analogy to the $CePd_3$ spectra [41,42] we assign the two sharp peaks near E_F to Ce $4f^1{}_{5/2}$, $4f^1{}_{7/2}$ (spin-orbit satellite) and the broad peak around 1.4–1.6 eV to $4f^0$. The broad maximum peak around 1.4–1.6 eV may include a tail of the surface contribution of the Ce $4f$ components as well as that of the Pd $4d$ components [42,43].

We should note here that these Ce $4f$ spectral features are totally different from the partial Ce $4f$ DOS, which is a clear indication of the significant electron correlation effects. In general, the angle-integrated photoemission spectral shape can be written as $\rho(\omega) \equiv \int dk A(k,\omega) = -\mathrm{Im} \int dk \frac{1}{\pi} \frac{1}{\omega - \omega_k^0 - \Sigma(k,\omega)}$, where ω_k^0 denotes the energy for the noninteracting band, and $\Sigma(k,\omega)$ is the electron self-energy [44,45]. If the electron correlation is not significant, the DOS given by the DFT should give a good estimate for ω_k^0 as well as $\rho(\omega)$. In the case of strongly correlated electron systems, however, the spectral function should be significantly different from the DOS due to the self-energy.

In order to explain the angle-integrated Ce $4f$ spectral features, the Anderson impurity model is usually employed [34,44,46]. The Anderson impurity model calculation can reproduce a broad f^0 peak at $E_b \sim 1.5$ eV and f^1 peak near E_F, which is actually a tail of the Kondo resonance peak located at $k_B T_K$ (T_K: Kondo temperature) above E_F.

Although we do not perform the Anderson impurity model calculation here, based on the reported results on various Ce compounds [44,46], we found a localized nature of the Ce $4f$ electrons because the f^0 weight is much stronger than the f^1 weight. This seems to be consistent with the magnetic susceptibility measurement for $Ce_3Pd_{20}Si_6$ showing the Ce charge state of nearly 3+ [1]. The Ce $3d$ core-level PES is desirable for $Ce_3Pd_{20}X_6$ to evaluate the exact valence state in the ground state.

In Fig. 8(a) the spectral weight of the Pd $4d$ component at $E_b \sim 2.5$ eV seems to decrease with decreasing temperature, similar to what we have shown for low photon energies [compare Figs. 7(a) and 7(b)]. However here the spectral feature lies on the tail of a strong f^0 component and may overlap with the $4f$ surface contribution. Therefore the low photon energy measurement gives more reliable information about the temperature dependence of the Pd $4d$-dominated valence band.

In Fig. 8(c) an expanded view of the valence-band spectra near E_F is shown as a function of the temperature. We observe a peak at $E_b \sim 0.28$ eV, which reflects the Ce $4f^1{}_{7/2}$ spectral feature. The temperature dependence of the resistivity showed the onset of the Kondo screening with a maximum at about 20 K [8]. We should observe the development of the pseudogap around the Fermi edge at low temperatures due to the hybridization [1,14]. However, the intensity of $4f^1{}_{5/2}$ in Fig. 8(c) only shows a weak temperature dependence because of the resolution broadening of 40 meV. High-resolution ARPES measurements of the valence-band spectra from single crystals remain future work.

Winkler *et al.* [6,7] concluded that the Ce ions at the (4a) site play a minor role in the incoherent Kondo scattering at high temperatures and Ce ions at the (8c) site have a higher Kondo temperature than those at the (4a) site. It is noted that our PES is not site selective and thus indicates a superposition of the valence-band spectra from the two distinct Ce sites.

In Figs. 9(a) and 9(b) we show the valence-band spectra of $Ce_3Pd_{20}Ge_6$ at 10 and 100 K. We do not see a significant temperature dependence. This result is reasonable because the Kondo temperature was estimated to be of the order of a few

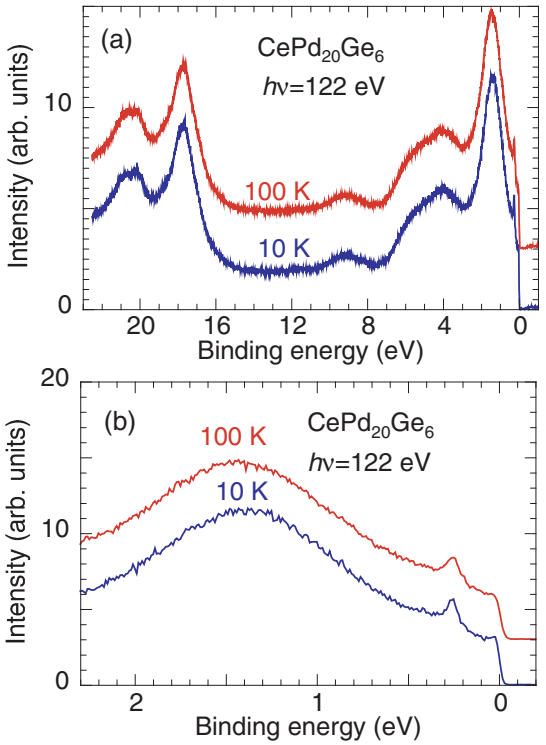

FIG. 9. (Color online) (a) Valence-band spectra at 10 and 100 K and $h\nu = 122$ eV for $Ce_3Pd_{20}Ge_6$. (b) Enlarged view of the valence-band spectra in (a) near E_F.

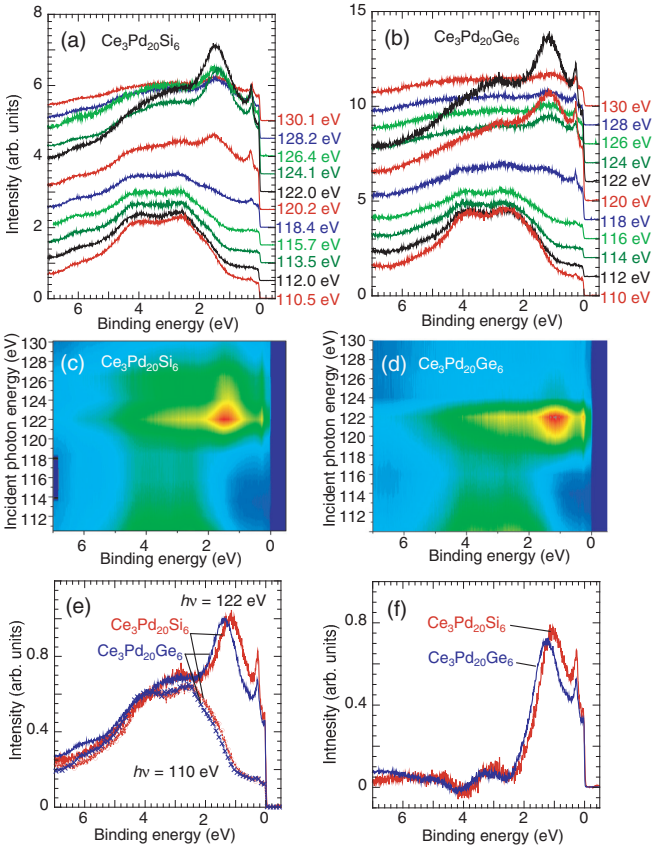

FIG. 10. (Color online) (a) Resonant photoelectron spectra of the valence band for $Ce_3Pd_{20}Si_6$ at 8 K in the incident energy range $h\nu = 110.5$–130.1 eV. (b) Resonant photoelectron spectra of the valence band for $Ce_3Pd_{20}Ge_6$ at 10 K in the incident energy range $h\nu = 110$-130 eV. (c) Contour intensity map of the resonant spectra in (a) as a function of the incident photon energies. (d) Contour intensity map of the resonant spectra in (b) as a function of the incident photon energies. (e) Comparison of the spectra at 110 eV (off resonance) and 122 eV (on resonance) for $Ce_3Pd_{20}Si_6$ and $Ce_3Pd_{20}Ge_6$. On-resonance spectra are normalized at 7 eV. The off-resonant spectra intensity is normalized to the intensity at 4 eV for on-resonance spectra. (f) Difference in the intensity between on- and of-resonant spectra for $Ce_3Pd_{20}Si_6$ and $Ce_3Pd_{20}Ge_6$.

kelvins [2], which is below the temperature measured in this experiment.

B. Resonant PES

Figures 10(a) and 10(b) show the valence-band spectra measured around $h\nu = 110$–130 eV for $Ce_3Pd_{20}Si_6$ and $Ce_3Pd_{20}Ge_6$, respectively, where the Ce $4d$-$4f$ resonance occurs. In Figs. 10(c) and 10(d) we show contour intensity maps as a function of the incident photon energies, where a strong enhancement of the intensity of the $4f^1$ and $4f^0$ components is observed at the $4d$-$4f$ resonance. This again confirms the assignment of these $4f$ components described above.

In Fig. 10(e) we show the spectra of on- and off-resonance for $Ce_3Pd_{20}Si_6$ and $Ce_3Pd_{20}Ge_6$. Figure 10(f) shows the intensity difference between spectra on- and spectra off-resonance. The off-resonant spectra do not show a significant difference between these two compounds. We should note, however, that the relative spectral intensity ratio f^1/f^0 for $Ce_3Pd_{20}Si_6$ is apparently stronger than that for $Ce_3Pd_{20}Ge_6$. This result indicates that the c-f hybridization of $Ce_3Pd_{20}Si_6$ is stronger than that of $Ce_3Pd_{20}Ge_6$. We assume that this is related to the enhanced electronic specific heat in $Ce_3Pd_{20}Si_6$. In order to analyze the Ce $4f$ spectra quantitatively, however, we need to separate the electronic states at (8c) and (4a) sites as well as the surface contribution.

V. CONCLUSION

We have performed detailed DFT calculations and high-resolution PES measurements for the heavy fermion compound $Ce_3Pd_{20}X_6$ (X = Si, Ge) in the UV and SX photon energy ranges and we were able to clarify both experimentally and theoretically the different contributions to the electronic structure.

The DFT calculation of the DOS was able to identify the main orbital contributions to the valence band and conduction band of these materials and shows an overall good agreement with the experimental valence-band spectra. By comparing calculated and experimental values of the electronic specific heat coefficient, we estimated the enhancement factors of $z^{-1} \sim 550$ for $Ce_3Pd_{20}Si_6$ and $z^{-1} \sim 37$ for $Ce_3Pd_{20}Ge_6$. We found that the electron correlation effect is significant not only for $Ce_3Pd_{20}Si_6$ but also for $Ce_3Pd_{20}Ge_6$. The orbital

decomposition of the electronic structure by DFT calculations indicates that the Ce atoms at the (8c) site surrounded by 16 Pd atoms have a tendency to be magnetic. Ce atoms at the (4a) site surrounded by 12 Pd and 6 X atoms, on the other hand, are more localized and paramagnetic.

Experimentally we have demonstrated that the valence-band spectra of $Ce_3Pd_{20}Si_6$, taken at low photon energies, show only a weak temperature dependence and are dominated by Pd d states. By the Ce $4d$-$4f$ resonance PES, we clearly revealed the Ce $4f$ states in the valence band close to the E_F of these compounds. We further observe a rather strong f^0 component with only a small fraction of f^1 component, indicating the localized nature of the $4f$ electrons. The relative intensity f^1/f^0 for $Ce_3Pd_{20}Si_6$ is stronger than that for $Ce_3Pd_{20}Ge_6$ at $4d$-$4f$ resonance, suggesting stronger c-f hybridization in the former. However, in order to analyze the Ce $4f$ spectra quantitatively, we need to separate the electronic states at (8c) and (4a) sites as well as the surface contribution.

The electrical resistivity and specific heat measurements have been performed on single-crystalline $Ce_3Pd_{20}Ge_6$ [47]. For single-crystalline $Ce_3Pd_{20}Si_6$ low-temperature elastic properties [12], magnetization at low temperatures down to 90 mK [13], specific heat measurements [17], and neutron scattering to determine the crystal-field levels [48] have been published. Our theoretical results may motivate de Haas–van Alphen or ARPES experiments on these single-crystalline samples in the future. We expect that this k-resolved information will benefit our further understanding of these compounds.

ACKNOWLEDGMENTS

The experiments were performed at HiSOR beamlines BL-1 and BL-9A (HiSOR under Proposal Nos. 11-A-10 and 12-A-1) at Hiroshima University. We thank the N-BARD, Hiroshima University, for supplying the liquid helium as well as P. Aebi for helpful discussion. E.F.S acknowledges financial support from the JSPS postdoctoral fellowship for overseas researchers as well as the Alexander von Humboldt Foundation (Grant No. P13783) and the Swiss National Foundation fellowship for prospective researchers (Grant No. PBFRP2_140028).

[1] N. Takeda, J. Kitagawa, and M. Ishikawa, New heavy-electron system $Ce_3Pd_{20}Si_6$, J. Phys. Soc. Jpn. **64**, 387 (1995).

[2] J. Kitagawa, N. Takeda, and M. Ishikawa, Possible quadrupolar ordering in a Kondo-lattice compound $Ce_3Pd_{20}Ge_6$, Phys. Rev. B **53**, 5101 (1996).

[3] A. M. Strydom, A. Pikul, F. Steglich, and S. Paschen, Possible field-induced quantum criticality in $Ce_3Pd_{20}Si_6$, J. Phys.: Conf. Ser. **51**, 239 (2006).

[4] S. Paschen, M. Müller, J. Custers, M. Kriegisch, A. Prokofiev, G. Hilscher, W. Steiner, A. Pikul, F. Steglich, and A. M. Strydom, Quantum critical behaviour in $Ce_3Pd_{20}Si_6$? J. Magn. Magn. Mater. **316**, 90 (2007).

[5] A. Prokofiev, J. Custers, M. Kriegisch, S. Laumann, M. Müller, H. Sassik, R. Svagera, M. Waas, K. Neumaier, A. M. Strydom, and S. Paschen, Crystal growth and composition-property relationship of $Ce_3Pd_{20}Si_6$ single crystals, Phys. Rev. B **80**, 235107 (2009).

[6] H. Winkler, S. Laumann, J. Custers, A. Prokofiev, and S. Paschen, Lu and La substituted $Ce_3Pd_{20}Si_6$, Phys. Status Solidi B **247**, 516 (2010).

[7] H. Winkler, K.-A. Lorenzer, S. Laumann, J. Custers, A. Prokofiev, and S. Paschen, Chemical pressure, dilution and disorder in the heavy fermion compounds $Ce_{3-x}La_xPd_{20}Si_6$ ($x = 1/3, 2/3$), J. Phys.: Condens. Matter **23**, 094208 (2011).

[8] J. Custers, K.-A. Lorenzer, M. Müller, A. Prokofiev, A. Sidorenko, H. Winkler, A. M. Strydom, Y. Shimura, T. Sakakibara, R. Yu, Q. Si, and S. Paschen, Destruction of the Kondo effect in the cubic heavy-fermion compound $Ce_3Pd_{20}Si_6$, Nature Mater. **11**, 189 (2012).

[9] T. Hashiguchi, N. Takeda, J. Kitagawa, N. Wada, S. Takayanagi, M. Ishikawa, and N. Mōri, Pressure effect on transport properties and specific heat of Kondo compound $Ce_3Pd_{20}Si_6$, J. Phys. Soc. Jpn. **69**, 667 (2000).

[10] H. Hidaka, S. M. Ramos, E. N. Hering, M. B. Fontes, E. B. Saitovitch, S. Otani, T. Wakabayashi, Y. Shimizu, T. Yanagisawa, and H. Amitsuka, Effects of pressure on cage-structural compound $Ce_3Pd_{20}Ge_6$, J. Phys. Conf. Ser. **391**, 012019 (2012).

[11] A. V. Gribanov, Yu. D. Seropegin, and O. I. Bodak, Crystal structure of the compounds $Ce_3Pd_{20}Ge_6$ and $Ce_3Pd_{20}Si_6$, J. Alloys Compd. **204**, L9 (1994).

[12] T. Goto, T. Watanabe, S. Tsuduku, H. Kobayashi, Y. Nemoto, T. Yanagisawa, M. Akatsu, G. Ano, O. Suzuki, N. Takeda, A. Dönni, and H. Kitazawa, Quadrupole ordering in clathrate compound $Ce_3Pd_{20}Si_6$, J. Phys. Soc. Jpn. **78**, 024716 (2009).

[13] H. Mitamura, T. Tayama, T. Sakakibara, S. Tsuduku, G. Ano, I. Ishii, M. Akatsu, Y. Nemoto, T. Goto, A. Kikkawa, and H. Kitazawa, Low temperature magnetic properties of $Ce_3Pd_{20}Si_6$, J. Phys. Soc. Jpn. **79**, 074712 (2010).

[14] Yu. P. Gaĭdukov, Yu. A. Koksharov, Yu. V. Kochetkov, I. Mirkovich, and V. N. Nikiforov, $Ce_3Pd_{20}(Ge)Si_6$: A new Kondo system? JETP Lett. **61**, 391 (1995).

[15] P. Y. Portnichenko, A. S. Cameron, M. A. Surmach, P. P. Deen, S. Paschen, A. Prokofiev, J.-M. Mignot, A. M. Strydom, M. T. F. Telling, A. Podlesnyak, and D. S. Inosov, Momentum-space structure of quasielastic spin fluctuations in $Ce_3Pd_{20}Si_6$, Phys. Rev. B **91**, 094412 (2015).

[16] H. Ono, T. Nakano, N. Takeda, G. Ano, M. Akatsu, Y. Nemoto, T. Goto, and H. Kitazawa, Specific heat of $Ce_3Pd_{20}Si_6$ single crystal in magnetic fields, J. Phys.: Conf. Ser. **391**, 012054 (2012).

[17] H. Ono, T. Nakano, N. Takeda, G. Ano, M. Akatsu, Y. Nemoto, T. Goto, A. Dönni, and H. Kitazawa, Magnetic phase diagram of clathrate compound $Ce_3Pd_{20}Si_6$ with quadrupolar ordering, J. Phys.: Condens. Matter **25**, 126003 (2013).

[18] S. Paschen and J. Larrea, Ordered phases and quantum criticality in cubic heavy fermion compounds, J. Phys. Soc. Jpn. **83**, 061004 (2014).

[19] J. Custers, P. Gegenwart, C. Geibel, F. Steglich, P. Coleman, and S. Paschen, Evidence for a non-Fermi-liquid phase in Ge-substituted $YbRh_2Si_2$, Phys. Rev. Lett. **104**, 186402 (2010).

[20] P. P. Deen, A. M. Strydom, S. Paschen, D. T. Adroja, W. Kockelmann, and S. Rols, Quantum fluctuations and the magnetic ground state of $Ce_3Pd_{20}Si_6$, Phys. Rev. B **81**, 064427 (2010).

[21] A. Dönni, T. Herrmannsdörfer, P. Fischer, L. Keller, F. Fauth, K. A. McEwen, T. Goto, and T. Komatsubara, Low-temperature antiferromagnetic moments at the 4a site in $Ce_3Pd_{20}Ge_6$, J. Phys.: Condens. Matter **12**, 9441 (2000).

[22] V. N. Duginov, K. I. Gritsaj, V. Yu. Pomjakushin, A. N. Ponomarev, A. A. Nezhivoy, A. V. Gribanov, V. N. Nikiforov, and Yu. D. Seropegin, A μSR study of the magnetic properties of $Ce_3Pd_{20}Ge_6$, Physica B: Condens. Matter **374–375**, 192 (2006).

[23] H. Harima, Electronic structure and Fermi surfaces of $La_3Pd_{20}Ge_6$, Physica B: Condens. Matter **281–282**, 775 (2000).

[24] T. Yamamizu, M. Nakayama, N. Kimura, T. Komatsubara, and H. Aoki, Magnetic phase diagram of $Ce_3Pd_{20}Ge_6$ under uniaxial pressure, Physica B: Condens. Matter **312-313**, 495 (2002).

[25] Y. Nemoto, T. Yamaguchi, T. Horino, M. Akatsu, T. Yanagisawa, T. Goto, O. Suzuki, A. Dönni, and T. Komatsubara, Ferroquadrupole ordering and Γ_5 rattling motion in the clathrate compound $Ce_3Pd_{20}Ge_6$, Phys. Rev. B **68**, 184109 (2003).

[26] T. Watanabe, T. Yamaguchi, Y. Nemoto, T. Goto, N. Takeda, O. Suzuki, and H. Kitazawa, Ultrasonic study of rattling and tunneling in clathrate compounds $R_3Pd_{20}X_6$ (R = La, Ce; X = Si, Ge), J. Magn. Magn. Mater. **310**, 280 (2007).

[27] H. Yamaoka, P. Thunström, I. Jarrige, K. Shimada, N. Tsujii, M. Arita, H. Iwasawa, H. Hayashi, J. Jiang, T. Habuchi, D. Hirayama, H. Namatame, M. Taniguchi, U. Murao, S. Hosoya, A. Tamaki, and H. Kitazawa, High-resolution photoelectron spectroscopy study of Kondo metals: $SmSn_3$ and $Sm_{0.9}La_{0.1}Sn_3$, Phys. Rev. B **85**, 115120 (2012).

[28] H. Yamaoka, P. Thunström, N. Tsujii, I. Jarrige, K. Shimada, M. Arita, H. Iwasawa, H. Hayashi, J. Jiang, H. Namatame, M. Taniguchi, N. Hiraoka, H. Ishii, K.-D. Tsuei, M. Giovannini, and E. Bauer, Electronic structure and the valence state of Yb_2Pd_2Sn and $YbPd_2Sn$ studied by photoelectron and resonant x-ray emission spectroscopies, Phys. Rev. B **86**, 085137 (2012).

[29] A. Dönni, H. Kitazawa, T. Strässle, L. Keller, M. Matsuda, K. Kakurai, G. Ano, M. Akatsu, Y. Nemoto, and T. Goto, Crystal field level diagrams at the Pr Sites (8c) and (4a) in the clathrate compound $Pr_3Pd_{20}Si_6$, J. Phys. Soc. Jpn. **80**, 044715 (2011).

[30] http://elk.sourceforge.net/.

[31] J. P. Perdew and Y. Wang, Accurate and simple analytic representation of the electron-gas correlation energy, Phys. Rev. B **45**, 13244 (1992).

[32] H. J. Monkhorst and J. D. Pack, Special points for Brillonin-zone integrations, Phys. Rev. B **13**, 5188 (1976).

[33] K. Yamada, *Electron Correlation in Metals* (Cambridge University Press, Cambridge, UK, 2004), Chap. 7.

[34] A. C. Hewson, *The Kondo Problem to Heavy Fermions* (Cambridge University Press, Cambridge, UK, 1993), Chap. 10.

[35] If $z \gg 1$, then $\rho_c \ll \frac{1}{z}\rho_f(E_F)$ and γ can be approximated by considering only the density of f states at E_F.

[36] Note that, similarly to Fig. 2, the spin- and site-resolved partial DOS is obtained by summing over the DOS of equivalent atoms in the unit cell.

[37] The image plot is obtained by calculating the d and f weight inside the muffin-tin of each Pd and Ce site at each k point along the high-symmetry path and adding a Gaussian function with $\sigma = 75$ meV and an area corresponding to the d and f weights centered at the eigenenergy of the band.

[38] K. Shimada, M. Arita, Y. Takeda, H. Fujino, K. Kobayashi, T. Narimura, H. Namatame, and M. Taniguchi, High-resolution, low-temperature photoemission spectroscopy at the HiSOR linear undulator beamline, Surf. Rev. Lett. **09**, 529 (2002).

[39] M. Arita, K. Shimada, H. Namatame, and M. Taniguchi, High-resolution, low-temperature photoemission spectroscopy at the HiSOR helical-undulator beamline, Surf. Rev. Lett. **09**, 535 (2002).

[40] J. J. Yeh and I. Lindau, Atomic subshell photoionization cross sections and asymmetry parameters: $1 \leqslant Z \leqslant 103$, At. Data Nucl. Data Tables **32**, 1 (1985).

[41] M. Zacchigna, J. Almeida, I. Vobornik, G. Margaritondo, D. Malterre, B. Malaman, and M. Grioni, High-resolution resonant photoemission study of the $4f$ states in a typical Kondo system: $CePd_3$, Eur. J. Phys. **2**, 463 (1998).

[42] S. Danzenbächer, Yu. Kucherenko, M. Heber, D. V. Vyalikh, S. L. Molodtsov, V. D. P. Servedio, and C. Laubschat, Wave-vector dependent intensity variations of the Kondo peak in photoemission from $CePd_3$, Phys. Rev. B **72**, 033104 (2005).

[43] M. Mulazzi, K. Shimada, J. Jiang, H. Iwasawa, and F. Reinert, Evidence of coexisting Kondo screening and valence fluctuations in the $CePd_7$/Pd(001) surface alloy, Phys. Rev. B **89**, 205134 (2014).

[44] S. Hüfner, *Photoelectron Spectroscopy*, 3rd ed. (Springer-Verlag, Berlin, 2003).

[45] G. Borstel, Theoretical aspects of photoemission, Appl. Phys. A **38**, 193 (1985).

[46] O. Gunnarsson and K. Schönhammer, in *Handbook on the Physics and Chemistry of Rare Earth*, edited by K. A. Gschneider, L. Eyring, and S. Hüfner (North-Holland, Amsterdam, 1987), Vol. 10, Chap. 64.

[47] J. Kitagawa, N. Takeda, M. Ishikawa, M. Nakayama, N. Kimura, and T. Komatsubara, Third-order magnetic susceptibility and quadrupolar order parameter of Kondo-lattice compound $Ce_3Pd_{20}Ge_6$, J. Phys. Soc. Jpn. **69**, 883 (2000).

[48] S. Paschen, S. Laumann, A. Prokofiev, A. M. Strydom, P. P. Deen, J. R. Stewart, K. Neumaier, A. Goukassov, and J.-M. Mignot, First neutron measurements on $Ce_3Pd_{20}Si_6$, Physica B **403**, 1306 (2008).